ISSN 1063-4576, Journal of Superhard Materials, 2021, Vol. 43, No. 1, pp. 12–20. © Allerton Press, Inc., 2021.
Ukrainian Text © The Author(s), 2021, published in Sverkhtverdye Materialy, 2021, Vol. 43, No. 1, pp. 17–28.

PRODUCTION, STRUCTURE, PROPERTIES

Phase Composition, Microstructure, and Wear Properties of Ni/Ni_3Si Composites Prepared by Mechanical Alloying

Junxi Zhang[a], *, Baiming Chen[a], Wu Yue[a], and Hui Chen

[a] *School of Materials Engineering, Lanzhou Institute of Technology, Lanzhou Gansu, 730050 China*

**e-mail: 57764866@qq.com*

Received June 11, 2019; revised November 14, 2019; accepted January 20, 2020

Abstract—Ni_3Si and Ni/Ni_3Si composites were prepared by mechanical alloying with Ni and Si powders as raw materials. The phase composition, microstructure and wear properties of the Ni_3Si and Ni/Ni_3Si composites were investigated. The results showed that the Ni (Si) solid solution, $Ni_{74}Si_{26}$ and $Ni_{31}Si_{12}$ intermediate phases were formed during ball milling process and then Ni_3Si nanocrystalline powder was produced after 30 h of milling. Based on Miedema's semi-empirical theory, the formation free energies of different phases formed during mechanical alloying of 3Ni–Si mixed powders were calculated. The results showed that the ordered phase of Ni_3Si is stable under equilibrium conditions and has the lowest formation enthalpy during ball milling. Compared with the monolithic Ni_3Si, the Ni/Ni_3Si composite has an excellent friction and wear resistance and comprehensive strength and toughness. With the increase of load, the friction coefficient of the composite decreases, the wear rate of the composite increases first and then decreases. When the load is 10 N, the friction coefficient and wear rate of the Ni/Ni_3Si composite are 0.246 and 5.23×10^{-4} $mm^3/(Nm)$, respectively. The main wear mechanism of the material experiences a transition from adhesive wear to abrasive wear with the increase of load, and exhibits a significant tribo-oxidation wear under all loads.

Keywords: metal silicides, hot pressing, microstructure, friction and wear behavior

DOI: 10.3103/S1063457621010081

INTRODUCTION

With the rapid development of aerospace technology, traditional nickel-based alloys cannot meet the requirements for high-temperature structural materials due to their high density and low operating temperature (≤1100°C). Metal silicide Ni_3Si is considered to be the most promising candidate material for high temperature structure under severe conditions due to its high melting point (T_m = 1523 K), high strength, low density, high specific modulus, excellent wear and corrosion resistance [1–3]. However, like most of the metal silicides, severe low temperature brittleness limits its practical application [4]. Some studies have shown that the high temperature strength, corrosion and friction and wear properties of Ni_3Si have been significantly improved by introducing Ti, Nb, B, Ta and other alloying elements to Ni_3Si. However, the room temperature toughening is limited due to the lack of key plastic toughening phases [5–7]. Refining matrix grains and compositing with a second phase is another effective method to improve the mechanical properties of metal silicides [8, 9]. Dyck et al. prepared Ni–Ni_3Si eutectic in-situ composites by arc melting and directional solidification techniques, respectively [10–12]. The composite is formed in situ and has the characteristics of high interfacial bonding strength and uniform distribution of the second phase. However, the limitation of these methods lies in that they have high requirements on equipment, complicated processes, microstructure stress and defects or the products are porous.

Mechanical alloying is basically a dry and high energy ball milling process which has been used to prepare metal silicides and composites with nanocrystalline structure [13]. However, the nanocrystalline structure obtained by mechanical alloying is easy to be damaged due to grain growth during high temperature sintering. Therefore, for nanocrystalline structural materials, it is necessary to control the grain growth during sintering [14]. Medium frequency induction hot-pressing method has a high-energy heat source for sintering simultaneously with a uniaxial pressure to primarily sinter powders. The sintered compact material can be obtained in a short period time at a relatively lower temperature. Many intermetallic compounds, ceramics and composites prepared by medium frequency induction hot press sintering have a high density and fine microstructure [15].

In this work, Ni_3Si nanocrystalline composite powders were prepared by mechanical alloying. The microstructure, phase composition and thermodynamics of the powders during ball milling were studied. Subsequently, Ni_3Si and Ni/Ni_3Si eutectic composites were prepared by hot pressing sintering. The phase transformation, microstructure and wear resistance of the Ni_3Si and Ni/Ni_3Si composite were also studied in details.

EXPERIMENTAL

The elemental powders of Ni (purity 99.5%, <200 mesh, Sinopharm Chemical Reagent Co. Ltd.) and Si (purity 99.9%, <200 mesh, Sinopharm Chemical Reagent Co. Ltd.) were used as starting materials. In order to obtain Ni_3Si and Ni/Ni_3Si eutectic composite, the proportion of 86.3Ni–13.7Si and 88.5Ni–11.5Si (wt %) was weighed and mixed together according to the binary phase diagram of Ni–Si. The mechanical alloying process was carried out in a high energy planetary ball mill (QM-3SP2) at room temperature under Ar atmosphere. The high hardened steel vials and GCr15 steel balls were used for ball milling. Ball to powder weight ratio and milling speed were 15 : 1 and 400 rpm, respectively. Meanwhile, based on Miedema's semi-empirical theory, the formation free energies of different phases formed during mechanical alloying of 3Ni–Si mixed powders were calculated. After 30 h of milling, the ball-milled mixture was placed in a graphite die and introduced into a vacuum induction hot pressing sintering furnace with a pressure of 25 MPa. The samples were sintered at 1100°C for 1 h and then cooled to room temperature in the furnace. Finally, the disc specimens with the diameter of 30 mm and thickness of 5 mm were obtained.

The relative density of sintered samples was measured using the Archimedes method. The Vickers hardness values of the specimens were measured by HVS-1000 microhardness tester, with a 500 gf load and a 15 s dwell time. The flexural strength and fracture toughness of the specimens were measured. The size of the rectangular specimens is 2 × 4 × 25 mm, and the span of the fixture is 20 mm. Before the wear test, the sintered samples were cut and polished by 1200# sandpaper, and then ultrasonically cleaned in acetone. Friction and wear experiments were carried out using a TE 70SLIM ball-on-disc fretting machine under dry conditions at room temperature in air with a relative humidity of 50–60%. During the wear test, the GCr15 steel ball (with a hardness of 5.8 GPa) was fretting on the specimen surface at 15 Hz oscillating frequency and 3 mm linear stroke for a duration time of 30 min under the applied normal loads of 2, 5, 7 and 10 N, respectively. Cross sections of worn scars of the specimens were measured using a surface profilometer (MicroXAM) after the wear tests. The wear volume and specific wear rate of the specimens were evaluated according to the following formula:

$$V = AL; \tag{1}$$

$$W = V/LN, \tag{2}$$

where V is the wear volume; A is area of the cross-section; L is the sliding distance; N is the normal load. The friction coefficient is automatically recorded by the friction and wear tester. The microstructure and phase composition of 3Ni–Si mixed powders and sintered samples were analyzed by means of D/Dmax-2400 X ray diffractometer. The microstructure and wear morphology of the composites were observed by OlypusBX51M metallographic microscope and JSM-6700F scanning electron microscope, and the chemical composition of the wear surface was determined by the energy dispersive spectrometer (EDS).

RESULTS

Structural Evolutions during Mechanical Alloying

X-ray diffraction patterns of 3Ni–Si mixed powders with different milling time are shown in Fig. 1. It can be seen that the sharp peaks from both Ni and Si for mixed powder after 0.5 h of milling. No chemical reaction occurred between the Ni and Si powders. With increase in the milling time, the diffraction peak of Si disappears and an amount of Si is dissolved in Ni to form Ni (Si) solid solution after 10 h of milling. At the same time, the ordered compound of Ni_3Si and the metastable phase of $Ni_{74}Si_{12}$ and $Ni_{31}Si_{12}$ were formed by the reaction between Ni and Si powder during mechanical alloying. After milling for 20 h, a portion of $Ni_{74}Si_{12}$ and $Ni_{31}Si_{12}$ metastable phases were transformed into Ni_3Si under the action of mechanical forces, which significantly increased the diffraction intensity of Ni_3Si. Finally, the single phase Ni_3Si powder was formed after milling for 30 h. Therefore, It can be concluded that the phase transition of the mixed powders occurs from 3Ni–Si powders to Ni (Si) solid solution, $Ni_{74}Si_{12}$ and $Ni_{31}Si_{12}$ metastable phase to Ni_3Si ordered compound with increasing milling time from 0.5 to 30 h.

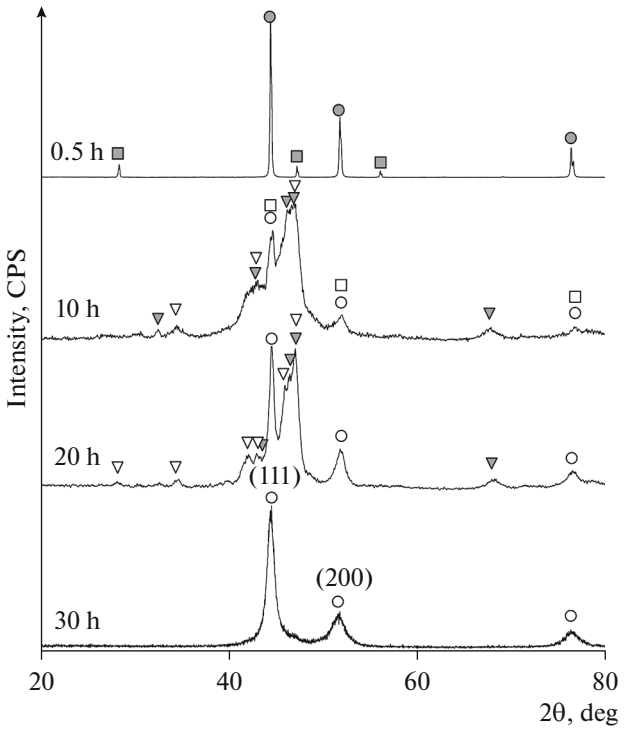

Fig. 1. XRD patterns of 3Ni–Si composite powder at different milling time: Ni (●), Si (■), Ni_{ss} (□), $Ni_{74}Si_{26}$ (▽), Ni_3Si (○), $Ni_{31}Si_{12}$ (▽).

The grain size and the lattice distortion of Ni_3Si phase were obtained from XRD analysis using the Williamson-Hall method [16]. According to the formula

$$B\cos\theta = 0.94\lambda/D + 3\varepsilon\sin\theta, \quad (3)$$

where D is the average grain size, λ is the X-ray wavelength, B is the FWHM of the diffraction peak, θ is the Bragg diffraction angle, ε is the lattice distortion. The grain size D and the lattice distortion ε of Ni_3Si phase can be calculated by introducing the B and λ values of (111) and (200) in the diffraction spectrum into the formula (3). The results showed that the grain size and lattice distortion of Ni_3Si were 52.3 nm and 0.76%, respectively, after 30 h of milling.

Microstructure and mechanical properties of sintered samples Ni_3Si and Ni/Ni_3Si composite were consolidated by hot pressing sintering of composite powders after 30 h of milling. The X-ray diffraction pattern of the sintered samples is shown in Fig. 2. It can be seen from Fig. 2, a that the main phase of the sintered sample at 1100°C is Ni_3Si using 3Ni–Si mixed powder as the initial material. The diffraction peaks of Ni and Si powders and other new phases were not found, which indicated that the reaction was complete under this condition. The main phase of $Ni–Ni_3Si$ eutectic composite is composed of Ni_3Si, Ni_{ss} and a small amount of $Ni_{31}Si_{12}$ phase, as shown in Fig. 2b. It has been proven that $Ni_{31}Si_{12}$ is a metastable phase, which can form Ni_3Si by annealing for a long time.

The microstructures of the products which were polished and etched using a solution of HNO_3 (4 vol %) and ethanol (96 vol %) was shown in Fig. 3. The Ni_3Si and Ni/Ni_3Si composite have a uniform and compact microstructure without obvious defects such as pores, inclusions and microcracks. The $Ni–Ni_3Si$ eutectic composite mainly consists of white matrix phase and gray grain boundary phase. Results of XRD (as shown in Fig. 2) and EDS analysis (the white phase: 86.71Ni–13.29Si, at % and gray boundary phase: 72.57Ni–25.43Si, at %) demonstrate that the white matrix phase is $Ni_{ss} + Ni_3Si$ and the grey grain boundary phase is $Ni_{ss} + Ni_{31}Si_{12}$. This is mainly due to the Ni/Ni_3Si mixed powder used in hot press sintering has higher sintering activity after 30 h of milling, thus reducing the sintering temperature. When sintered at 1100°C (which is close to the melting point of Ni/Ni_3Si eutectic about 1143°C), a part of low-melting liquid phase structure is formed at the grain boundary. During the subsequent cooling process, the high melting point of Ni precipitated from the grain boundary liquid phase firstly, which results the Si content

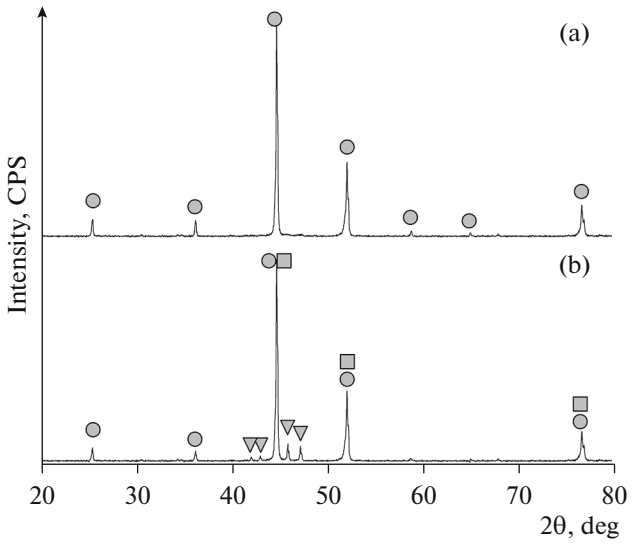

Fig. 2. XRD patterns of hot-pressed samples Ni_3Si (a) and Ni/Ni_3Si (b) composite; Ni_3Si (●), Ni_{ss} (□), $Ni_{31}Si_{12}$ (▽).

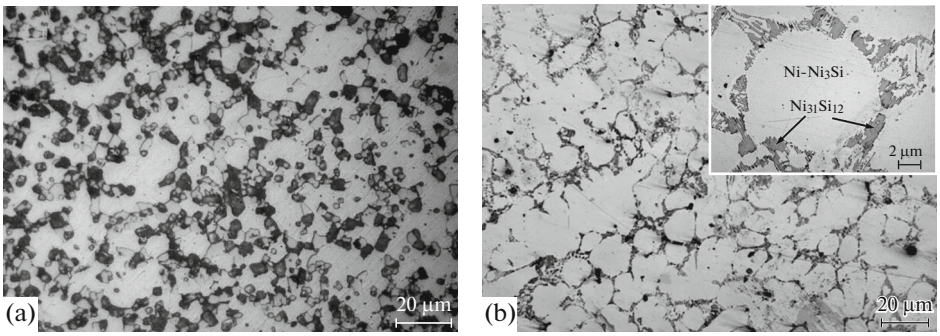

Fig. 3. Microstructure photograph of sintered samples Ni_3Si (a) and Ni/Ni_3Si (b) composite.

increased in the grain boundary residual liquid phase and the formation of metastable $Ni_{31}Si_{12}$ metal silicide. The metastable $Ni_{31}Si_{12}$ cannot be completely transformed into a stable Ni_3Si phase due to the rapid solidification process. Thereby, a metastable eutectic irregular structure Ni_{ss} + $Ni_{31}Si_{12}$ is formed at the grain boundary as shown in Fig. 3b.

The mechanical properties of Ni_3Si and Ni/Ni_3Si composite are shown in Table 1. According to Table 1, sintered samples have high sintering compactness, which is mainly attributed to the grain boundary liquid phase promoting the sintering densification. Compared with Ni_3Si alloy, Ni/Ni_3Si composite has higher sintering compactness, and its relative density is about 98.5%. Ni/Ni_3Si composite has a good combination of strength and toughness due to the high hardness of metal silicides Ni_3Si and $Ni_{31}Si_{12}$ and the toughening effect of Ni_{ss}. The hardness, flexural strength and fracture toughness of Ni/Ni_3Si composite was 6.68 GPa, 741 MPa and 8.92 MPa $m^{1/2}$, respectively.

Table 1. Mechanical properties of Ni_3Si and Ni/Ni_3Si composite

Material	Relative density, %	Hardness, GPa	Flexural strength, MPa	Fracture toughness, MPa $m^{1/2}$
Ni_3Si	98.0	6.97	624	5.47
Ni/Ni_3Si composite	98.5	6.68	741	8.92

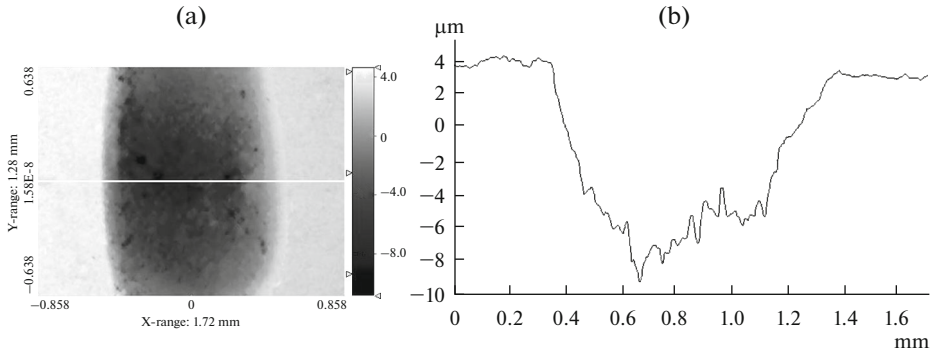

Fig. 4. The optical profile (a) and cross-sectional profile (b) of the wear scar on the Ni/Ni_3Si composite at 10 N load.

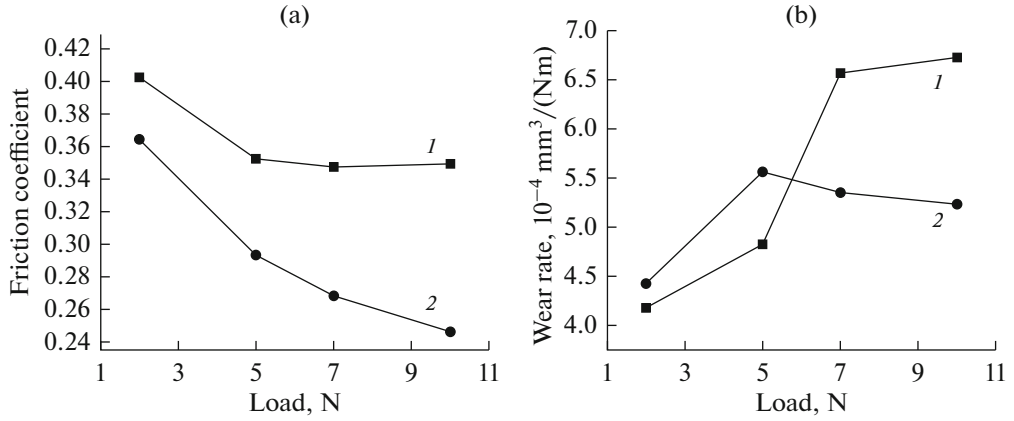

Fig. 5. Variation curve of friction coefficient (a) and wear rate (b) of Ni_3Si (*1*) and Ni/Ni_3Si (*2*) composite under different loads.

Friction and Wear Properties of the Sintered Samples

The sliding of the Ni_3Si and Ni/Ni_3Si composite against GCr15 steel balls led to significant wear of the samples (Fig. 4). The worn depths were observed to be in the range of 8–12 μm. The calculated specific friction coefficient and wear rate of Ni_3Si and Ni/Ni_3Si composite sliding against GCr15 steel balls under different loads are presented in Fig. 5. It is noted that the friction coefficient of Ni_3Si and Ni/Ni_3Si composite decreases with the increase of load. Compared with Ni_3Si alloy, the Ni/Ni_3Si composite exhibits a low coefficient friction under each load applied. The friction coefficient of Ni/Ni_3Si composite under 10 N load is about 0.246, which is 35% lower than that of Ni_3Si (as shown in Fig. 5a).

As shown in Fig. 5b, Ni_3Si and Ni/Ni_3Si composite exhibited outstanding wear resistant properties and low wear rate under room temperature dry-fretting wear test conditions against the GCr15 steel ball. The wear rate of Ni_3Si increases with the increase of load. The wear rate of Ni/Ni_3Si composite increases first and then decreases. The maximum wear rate of Ni/Ni_3Si composite is about 5.56×10^{-4} mm^3/(Nm) when the load is 5 N. The wear rate of Ni/Ni_3Si composite is considerably lower than that of the Ni_3Si alloy under the higher test load. When the load is 10 N, the wear rate of Ni/Ni_3Si composite is only 5.23×10^{-4} mm^3/(Nm), which is 25% lower than that of the single phase Ni_3Si.

DISCUSSIONS

Analysis of Mechanical Alloying Process

Based on the above experimental results, nanocrystalline Ni_3Si powder can be obtained by high energy ball milling using Ni and Si powders as raw materials. Mechanical alloying is a chemical solid-state reaction process, and the diffusion of components plays an important role in the formation of different phases

Table 2. Calculation results of ΔH and ΔG of 3Ni–Si powder in different states during ball milling process

Parameter	Intermetallic compound	Solid solution	Amorphous
ΔH, kJ mol^{-1}	–615.07	–68.72	–372.13
ΔG, kJ mol^{-1}	–615.07	–62.31	–363.79

in the solid state. According to the previous research results [17], there are two main reaction mechanisms in the mechanical alloying process:

– the new phases are formed by the mutual diffusion of the components, and the structures of the products tend to be disordered with the increase of milling time;

– suddenly formation of the products in a short period of milling time, which is similar to the mechanically alloyed self-sustaining reaction.

In this study, according to the XRD diffraction results of Fig. 1, the products $Ni_{74}Si_{26}$, $Ni_{31}Si_{12}$ and Ni_3Si phases were gradually formed by interdiffusion between the components. With the process of ball milling, the intermediate phase of $Ni_{74}Si_{26}$ and $Ni_{31}Si_{12}$ was first formed. After milling for 30 h, the intermediate phase $Ni_{74}Si_{26}$ and $Ni_{31}Si_{12}$ reacted with the residual components to form Ni_3Si according to the reactions

$$Ni_{31}Si_{12} + 5Ni = 12Ni_3Si; \quad (4)$$

$$3Ni_{74}Si_{36} + 2Si = 74Ni_3Si. \quad (5)$$

However, this is inconsistent with the results of Dyck et al. [10], which suggests that only Ni-based solid solution can be obtained by mechanical alloying. In order to further determine the phase composition of the product, the formation of enthalpy and free energy of the ordered intermetallic compound, solid solution and amorphous state of 3Ni–Si powder during mechanical milling was calculated by miedema semi-empirical theory [18]. The calculated temperature was 298 K. The results are shown in Table 2. It can be seen that 3Ni–Si powders are more inclined to form ordered intermetallic compound during mechanical milling because of the lower formation enthalpy and free energy of the system. The solid solution and amorphous metastable phase formed are mainly due to the mechanical alloying being a non-equilibrium preparation method, which causes the large lattice defects and surface free energy of the powder during the ball milling process. In addition, Ni is ferromagnetic, while Ni_3Si is not ferromagnetic. The magnetic properties of the powders with different milling time were analyzed. The results showed that the ferromagnetism of the powders decreased with the increase of milling time. The powders have no ferromagnetism after 30 h of milling, and it was estimated that the Ni_3Si phase was formed.

Wear Mechanisms of the Sintered Samples

In general, the wear resistance of a material is directly proportional to its hardness and fracture toughness according to the formula [19]

$$W \propto K_{Ic}^{-3/4} H^{-1/2}, \quad (6)$$

where H is the hardness of the materials; K_{Ic} is fracture toughness. According to Table 2, Ni/Ni_3Si composite has a good combination of hardness and fracture toughness due to the synergistic effect of the strengthening phase (Ni_3Si and $Ni_{31}Si_{12}$) and the ductile phase (Ni_{ss}). Therefore, the low wear rate is mainly attributed to the good combination of hardness and fracture toughness of Ni/Ni_3Si composite.

Wear failure of the material is related to the material parameters (hardness and toughness), operating parameters (load, sliding velocity, humidity and temperature) and its physical and chemical properties during the wear process. The results of Chen et al. indicated that the friction coefficient depended on the real contact area, the contact state and the lubricating role of debris [20]. The friction coefficient of the material increases under higher normal loads according to this theory. However, in our present work, a decrease of friction coefficient with load is observed. This may result from the generation of a lubricating surface layer through tribochemical reactions at higher loads. Figure 6 shows the wear morphology of Ni_3Si and Ni/Ni_3Si composite under different loads. It can be seen that the Ni_3Si and Ni/Ni_3Si composite have similar wear surface morphology and exhibit a distinct adhesive wear under low load (2 N). According to the results of EDS analysis, the main components of the adhesive layer on the worn surface are Fe, Ni, Si and O elements, as shown in Table 3. The presence of O element indicates the tribo-oxidation of

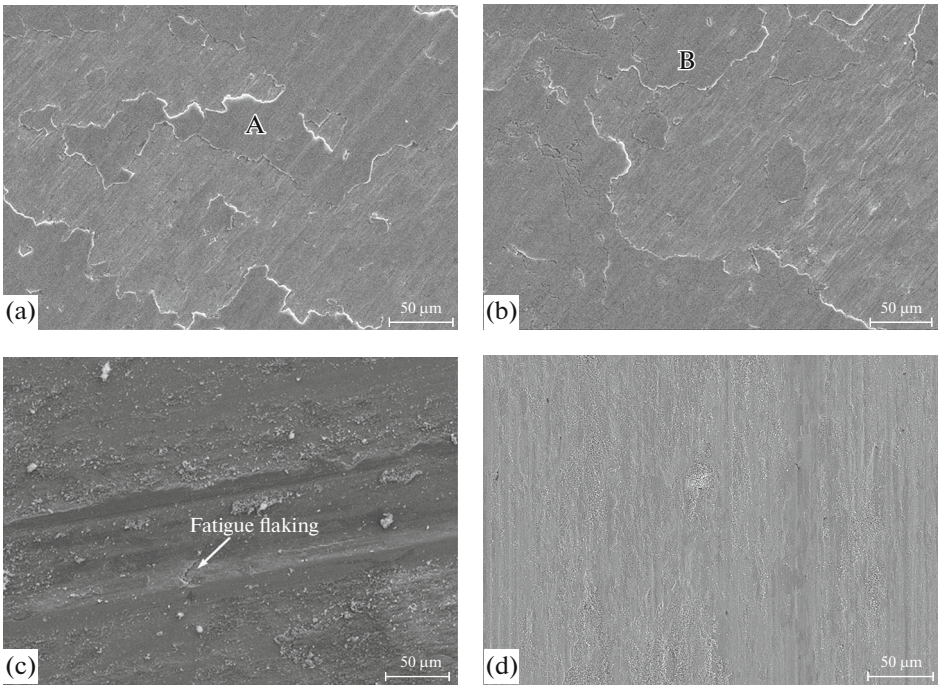

Fig. 6. Wear morphology of Ni_3Si (a, b) and Ni/Ni_3Si (c, d) composites under different loads: 2 N (a, c) and 10 N (b, d).

the experimental materials and the transfer of Fe oxide from steel ball. The material transfer from steel is probably due to the reduction of shear strength of GCr15 bearing steel balls under the effect of friction heat. Therefore, adhesion and tribo-oxidation are the main wear mechanisms of Ni_3Si and Ni/Ni_3Si composite under lower load. With the increase of load (10 N), the Ni_3Si and Ni/Ni_3Si composite exhibit an evident abrasive wear characteristics. The wear surface becomes smooth under the grinding of fine abrasive particles, as shown in Figs. 6c, 6d.

In addition, tribo-oxidation wear was observed at all loads. An important factor largely controlling the reported tribological behavior of metal silicides and its composites is their interaction with the atmosphere to form tribochemical oxides [21]. In particular, tribochemical wear will occur preferentially like in metals under unlubricated conditions of dry sliding. XRD analysis of the worn surface of Ni/Ni_3Si composite after fretting at 10 N loads is shown in Fig. 7. It can be noted that the SiO_2, NiO and Fe_2O_3 are detected on the fretting scar in addition to the matrix phases of Ni_{ss}, Ni_3Si and $Ni_{31}Si_{12}$. On the one hand, the formation of SiO_2, NiO and Fe_2O_3 phases with lubrication and prevent adhesive contact between the composite and steel balls, which result in reduction in friction coefficient and wear rate. On the other hand, for the brittle Ni_3Si materials, high load and cyclic stress also promote the initiation of cracking and subsequent brittle fracture and removal on the wear surface, which aggravates fatigue wear and increases the wear rate, as shown in Fig. 6c. It is explained that the Ni_3Si has a low friction coefficient and high wear rate under high load. Ni/Ni_3Si composite has a better wear resistance compared with single-phase Ni_3Si materials. For Ni/Ni_3Si composite, according to the Archard wear formula [22]

$$v = \frac{KWx}{H}, \tag{7}$$

Table 3. EDS analysis results of wear surface

Worn surface	Elements, at %			
	Ni	Si	Fe	O
Dot A in Fig. 6a	20.15	5.12	49.82	24.91
Dot B in Fig. 6b	27.88	4.67	43.37	23.08

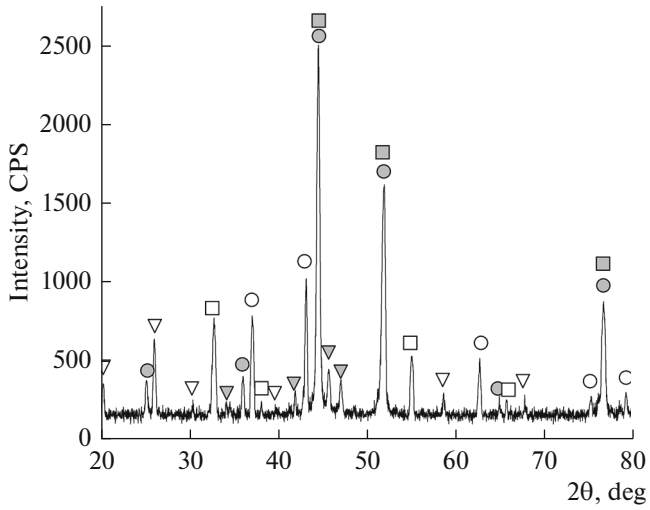

Fig. 7. XRD pattern of wear surface of Ni/Ni_3Si composite under 10 N load: Ni_3Si (●), Ni_{ss} (■), $Ni_{31}Si_{12}$ (▼), NiO (○), SiO_2 (▽), Fe_2O_3 (□).

where v is the wear volume; K is the friction coefficient; W is the applied load; x is the sliding distance; H is the hardness of the material. Obviously, low hardness and high friction coefficient will lead to high wear volume. However, in the present study, the wear rate of Ni/Ni_3Si composite is inversely proportional to its hardness. This can be attributed to the fact that in addition to hardness, the wear properties of the material also depend on its fracture toughness and friction coefficient according to formulas (5) and (6). Therefore, Ni/Ni_3Si composite has a good wear resistance compared with single-phase Ni_3Si materials due to its high hardness and fracture toughness and low friction coefficient.

CONCLUSIONS

The Ni_3Si nanocrystalline powder was synthesized by mechanical alloying using 3Ni–Si powder mixture as raw material. During the mechanical alloying, the Ni (Si) solid solution, $Ni_{74}Si_{26}$ and $Ni_{31}Si_{12}$ metastable phase was formed and then Ni_3Si nanocrystalline powder was produced after 30 h of milling. The microstructure of the Ni/Ni_3Si eutectic composite consists of Ni_3Si, Ni-based solid solution (Ni_{ss}) and a small amount of $Ni_{31}Si_{12}$ phase. Based on Miedema's semi-empirical theory, the formation free energies of different phases formed during mechanical alloying of 3Ni–Si mixed powders were calculated. The results showed that the ordered phase of Ni_3Si is stable under equilibrium conditions and has the lowest formation enthalpy during ball milling. Compared with the monolithic Ni_3Si, Ni/Ni_3Si composite exhibited an excellent combination of mechanical properties. The hardness, flexural strength and fracture toughness are 6.68 GPa, 741 MPa and 8.92 MPa $m^{1/2}$, respectively. Ni/Ni_3Si composite has a good wear resistance compared with single-phase Ni_3Si materials due to its high hardness and fracture toughness and low friction coefficient. The friction coefficient and wear rate of Ni/Ni_3Si composite is only 0.246 and 5.23×10^{-4} $mm^3/(Nm)$ at 10 N load, which is 35 and 25% lower than that of the monolithic Ni_3Si, respectively. The main wear mechanism of the material experiences a transition from adhesive wear to abrasive wear with the increase of load, and exhibits a significant tribo-oxidation wear under all loads.

ACKNOWLEDGMENTS

The authors acknowledge Ms Shaoyu Shi and Ms Qiuxiang Song for their assistance on experiments of hot press sintering and wear tests.

FUNDING

This research was supported by the Natural Science Foundation of Shandong Province of China (grant no. ZR2018MEM005).

REFERENCES

1. Semboshi, S., Takeuchi, T., Kaneno, Y., Iwase, A., and Takasugi, T., Thermal conductivity of Ni_3(Si,Ti) single-phase alloys, *Intermetallics*, 2018, vol. 92, pp. 119–125.
2. Gogebakan, M., Kursun, C., Gunduz, K.O., Tarakci, M., and Gencer, Y., Microstructural and mechanical properties of binary Ni–Si eutectic alloys, *J. Alloys Compd.*, 2015, vol. 643, no. 1, pp. 219–225.
3. Wei, L.F., Zhao, Z.L., Gao, J.J., and Cui, K., Morphological instability of lamellar structures in directionally solidified Ni–Ni_3Si alloys, *J. Cryst. Growth*, 2018, vol. 483, pp. 275–280.
4. Chen, H., Microstructure and mechanical properties of Mo_2Ni_3Si–Al_2O_3 nanocomposite synthesized by mechanical alloying, *J. Mater. Res.*, 2016, vol. 31, no. 21, pp. 3352–3359.
5. Gadang, P., Sanat, W., Kenji, O., Akihiro, I., and Takayuki, T., The environment-induced cracking of as-cold rolled Ni_3(Si,Ti) and Ni_3(Si,Ti) with 2Mo in sodium chloride solutions, *J. Alloys Compd.*, 2015, vol. 639, pp. 504–510.
6. Jang, J.S.C. and Tsau, C.H., The effect of niobium additions on the fracture of Ni–19Si-based alloys, *Mater. Sci. Eng., A*, 1992, vol. 153, nos. 1–2, pp. 525–531.
7. Imajo, D., Kaneno, Y., and Takasugi, T., Effect of Ta substitution method on the mechanical properties of Ni_3(Si,Ti) intermetallic alloy, *Mater. Sci. Eng., A*, 2013, vol. 588, pp. 228–238.
8. Chen, H., Shao, X., Wang, C.Z., Pu, X.P., Ma, J., and Huang, B.X., Effect of Al_2O_3 and Cu on the microstructure and oxidation properties of Mo_5Si_3 composite, *Corros. Sci.*, 2015, vol. 94, pp. 129–134.
9. Guan, K., Jia, L.N., Kong, B., Yuan, S.N., and Zhang, H., Study of the fracture mechanism of Nb_{SS}/Nb_5Si_3 in situ composite: based on a mechanical characterization of interfacial strength, *Mater. Sci. Eng., A*, 2016, vol. 663, pp. 98–107.
10. Dyck, S.V., Delaey, L., and Froyen, L., Reactive powder metallurgy of Ni,Si-based alloys, *Intermetallics*, 1995, vol. 3, no. 4, pp. 309–314.
11. Chang, F.E., Zhao, Z.W., Zhu, M., Li, N., Fang, W., Dong, G.Z., and Jian, Z.Y., Solidification behaviors of highly undercooled Ni–21.4%Si eutectic alloy, *Acta Metall. Sin.*, 2012, vol. 48, no. 7, pp. 875–881.
12. Cui, C.J., Zhang, J., Wu, K., Ma, Y.P., and Fu, H.Z., Microstructure and properties of Ni–Ni_3Si composites by directional solidification, *Phys. B* (Amsterdam), 2012, vol. 407, no. 17, pp. 3566–3569.
13. Zakeri, M., Yazdani-Rad, R., Enayati, M.H., and Rahimipoor, M.R., Synthesis of $MoSi_2$–Al_2O_3 nanocomposite by mechanical alloying, *Mater. Sci. Eng., A*, 2006, vol. 430, pp. 185–188.
14. Chen, H., Ma, Q., Shao, X., Ma, J., Wang, C., and Huang, B., Microstructure, mechanical properties and oxidation resistance of Mo_5Si_3–Al_2O_3 composite, *Mater. Sci. Eng., A*, 2014, vol. 592, pp. 12–18.
15. Chen, H., Ma, Q., Shao, X., Ma, J., and Huang, B.X., Corrosion and microstructure of the metal silicide $(Mo_{1-x}Nb_x)_5Si_3$, *Corros. Sci.*, 2013, vol. 70, pp. 152–160.
16. Ramezanalizadeh, H. and Heshmati-Manesh, S., Preparation of $MoSi_2$–Al_2O_3 nano-composite via MASHS route, *Int. J. Refract. Met. Hard Mater.*, 2012, vol. 31, pp. 210–217.
17. Anvari, S.Z., Karimzadeh, F., and Enayati, M.H., Synthesis and characterization of NiAl–Al_2O_3 nanocomposite powder by mechanical alloying, *J. Alloys Compd.*, 2009, vol. 477, pp. 178–181.
18. Chattopadhyay, C., Prasad, A., and Murty, B.S., Phase prediction in high entropy alloys—A kinetic approach, *Acta Mater.*, 2018, vol. 153, pp. 214–225.
19. Xu, J., Li, Z., Xie, Z.-H., Munroe, P., Lu, X.L., and Lan, X.F., Novel high damage-tolerant, wear resistant $MoSi_2$-based nanocomposite coatings, *Appl. Surf. Sci.*, 2013, vol. 270, pp. 418–427.
20. Chen, H., Shao, X., Wang, C.Z., Pu, X.P., Zhao, X.C., Huang, B.X., and Ma, J., Mechanical and wear properties of Mo_5Si_3–Mo_3Si–Al_2O_3 composites, *Intermetallics*, 2017, vol. 85, pp. 15–25.
21. Murthy, T.S.R.C., Basu, B., Srivastava, A., Balasubramaniam, R., and Suri, A.K., Tribological properties of TiB_2 and TiB_2–$MoSi_2$ ceramic composites, *J. Eur. Ceram. Soc.*, 2006, vol. 26, pp. 1293–1300.
22. Xu, J., Xie, Z.-H., and Munroe, P., Effect of Cr alloying on friction and wear of sputter-deposited nanocrystalline $(Mo_xCr_{1-x})_5Si_3$ films, *Intermetallics*, 2011, vol. 19, pp. 1146–1156.